Nanoscale corrosion analysis via in-situ surface potential mapping
Enhancing electrochemical insight with OL-EPM and AC-KPFM

Rahimi, Ehsan

DOI
10.1016/j.coelec.2025.101763

Publication date
2025

Document Version
Final published version

Published in
Current Opinion in Electrochemistry

Available online at www.sciencedirect.com

ScienceDirect

Current Opinion in Electrochemistry

Review Article

Nanoscale corrosion analysis via in-situ surface potential mapping: Enhancing electrochemical insight with OL-EPM and AC-KPFM

Ehsan Rahimi

Local nanoscale mapping of electrostatic surface potential (ESP) is advancing rapidly to meet the needs of electrochemistry and corrosion science. Conventional Kelvin probe force microscopy (KPFM), while valuable, is limited in liquid and dynamic redox environments due to restricted electrochemical control and spatial resolution. Recent advances in alternating current KPFM (AC-KPFM) and open-loop electric potential microscopy (OL-EPM) provide high-resolution, in-situ ESP imaging while suppressing parasitic Faradaic reactions. AC-KPFM is powerful for probing ionization and counterion interactions at solid–liquid interfaces, whereas OL-EPM enables visualization of corrosion initiation, nanoscale defects in coatings, and gradients across grain boundaries. Together, these methods bridge the gap between surface electrostatics and electrochemistry. Key challenges remain in temporal resolution, minimizing probe perturbations, and linking nanoscale data to macroscopic corrosion behavior. Nonetheless, these techniques reveal hidden electrochemical heterogeneities, clarify pathways of localized corrosion, and offer insights for designing durable, corrosion-resistant materials.

Addresses
Department of Materials Science and Engineering, Faculty of Mechanical Engineering (ME), Delft University of Technology, Mekelweg 2, 2628 CD, Delft, the Netherlands

Corresponding author: Rahimi, Ehsan (e.rahimi-2@tudelft.nl)

Current Opinion in Electrochemistry 2025, **54**:101763

This review comes from a themed issue on **Physical & Nano- Electrochemistry (2025)**

Edited by **Prof. Magdaléna Hromadová**, **Prof. Ismael Díez-Peréz**

For a complete overview see the Issue and the Editorial

Available online 1 October 2025

https://doi.org/10.1016/j.coelec.2025.101763

Introduction

The electrostatic surface potential (ESP) landscape at material interfaces, especially metals and alloys, governs essential phenomena in corrosion, catalysis, and energy conversion systems [1,2]. Spatial heterogeneity, stemming from surface films (oxide film or organic and inorganic nano-film), second phases, grain boundaries, or local defects (e.g., pores, inclusions, etc), can dramatically influence the onset of degradation or electrochemical reactivity [3]. Yet, traditional direct current (DC) electrochemical tools such as open-circuit potential (OCP) or potential vs. time (E vs. t) measurements and potentiodynamic polarization or current vs. voltage (I vs. V) are inherently limited by their macroscopic nature, averaging out critical local information [4]. This gap has motivated the adoption of scanning probe techniques capable of resolving ESP at the nanoscale under realistic electrochemical conditions [5].

Kelvin probe techniques measure the contact potential difference (CPD) between a conductive probe and a sample. CPD arises from differences in vacuum work function, making it a direct probe of local electronic properties at interfaces [6]. The macroscopic scanning Kelvin probe (SKP) implements this principle with a vibrating probe and conductive sample, yielding non-contact, area-averaged CPD maps at millimeter to micrometer scales [7,8]. However, SKP resolution is fundamentally limited, and its performance deteriorates under immersed conditions due to electrical noise, capacitive coupling, dipole screening, and parasitic electrolysis [9,10]. To overcome these constraints, Kelvin probe force microscopy (KPFM), an atomic force microscopy (AFM)-based variant, has been employed to resolve CPD at the nanometer scale [11]. In KPFM, the AFM tip acts as a nanoscale vibrating electrode: an applied electrical bias between tip and sample is adjusted to nullify the electrostatic force, allowing CPD measurement with nanometer-scale resolution. Critically, KPFM enables simultaneous mapping of surface topography and ESP, providing insight into local work function variation, charge distribution, and electronic heterogeneity [12,13].

KPFM has been applied extensively to semiconductors, thin films, energy materials, and metal alloys to study work function variation, electronic heterogeneity, and charge trapping. In corrosion studies, ex-situ KPFM has been used to map ESP differences between intermetallic particles and matrix phases in aluminum [14–16]

and magnesium alloys [17–19], carbon steels/stainless steel [20–22], identifying passive film evolutions [23,24], study environmental aging effects [25], and biological soft matter on biodegradation [26–28]. However, dry or ambient KPFM conditions do not support the electrochemical double layer formation, and therefore cannot directly reflect the effect of redox reactions on ESP mapping, and they are also limited in liquid environments, similar to SKP [25]. In response, recent advances in in-situ KPFM, notably open-loop electric potential microscopy (OL-EPM) and alternating current-KPFM (AC-KPFM), now allow researchers to perform non-invasive ESP mapping directly in liquid media, including corrosive environments. These techniques bypass several limitations of traditional DC-bias KPFM [5], offering new insights into corrosion initiation and surface degradation under realistic conditions due to local potential evolutions.

This mini-review highlights recent advances in *in-situ* nanoscale ESP mapping, with a particular focus on OL-EPM and AC-KPFM techniques as applied to electrochemistry and corrosion science. After a brief overview of OL-EPM and AC-KPFM technical foundations, five representative systems are presented to illustrate the unique capabilities of these methods in visualizing the influence of localized redox reactions on ESP imaging at the nanoscale.

Technical foundation: OL-EPM and AC-KPFM

Conventional KPFM employs a DC bias to nullify the electrostatic force between tip and sample [29]. In liquid or high-ionic-strength environments, however, this DC component induces parasitic electrochemical reactions, ion migration, and gas evolution, severely compromising measurement stability [10]. To overcome these limitations, OL-EPM and AC-KPFM avoid DC bias application, enabling non-invasive electrostatic measurements even in aqueous conditions.

OL-EPM applies a single high-frequency AC voltage between the tip and sample [30]. The resulting cantilever oscillations at frequency (ω) and its harmonic 2ω are used to derive local ESPs, eliminating the need for a feedback loop. In dual-frequency operation, additional mixed-frequency signals (e.g., $|\omega_1 - \omega_2|$) further enhance sensitivity and spatial resolution. Since no low-frequency components are involved, OL-EPM effectively suppresses electrochemical artifacts.

AC-KPFM, by contrast, replaces the conventional DC bias with a second AC component at twice the frequency [10]. The combined excitation, $U_C = a \cdot sin(\omega t) + b \cdot cos(2\omega t)$, is tuned such that the electrostatic force at ω is canceled ($F_\omega = 0$). Under this condition, the local ESP (ϕ) is determined directly from the amplitude (b), where $\phi = b/2$. As no DC voltage is applied, AC-KPFM is inherently immune to Faradaic processes and can be reliably operated in aqueous or reactive environments. Together, OL-EPM and AC-KPFM offer robust alternatives to conventional KPFM for high-resolution, quantitative ESP mapping in liquid and biological systems, without inducing electrochemical side effects. Table 1 summarizes how factors such as the measurement environment, probe size, feedback mechanism, and experimental limitations affect the performance of each technique and the interpretation of ESP measured using classical SKP, KPFM, AC-KPFM, and OL-EPM.

Applications of AC-KPFM and OL-EPM in electrochemistry and corrosion studies

This section highlights representative applications of AC-KPFM and OL-EPM, demonstrating how these techniques provide high-resolution, in-situ mapping of ESP distribution, enable real-time visualization of corrosion initiation, and reveal nanoscale electrochemical heterogeneities in diverse materials.

Ionization and counterion interactions at the Solid–Liquid interface using AC-KPFM

Understanding the evolution of surface charge at solid–liquid interfaces is critical for applications in energy conversion, biomaterials, and corrosion inhibition using organic molecules [31,32]. AC-KPFM enables precise mapping of nanoscale surface charge distributions, but its performance in liquid environments is strongly influenced by lift height and ionic screening.

In a landmark study, Hackl et al. investigated the ESP distribution of charged alkanethiol self-assembled monolayers (SAMs) on gold and examined how their ionization state varies with pH using AC-KPFM (Figure 1a and b) [10]. They observed that ESP signals decay with increasing tip–sample distance, with distinct behaviors in air and water. In air, contrast decreases gradually and remains detectable up to ~1.5 μm, whereas in deionized water, the signal decays exponentially and becomes negligible beyond ~1 μm due to ionic screening in the electrical double layer (Figure 1c and d). These results emphasize that maintaining minimal lift heights (<500 nm) is essential for reliable, high-resolution ESP mapping in electrolytic environments. This study highlights AC-KPFM's ability to correlate ESP variations with chemical ionization states while also demonstrating the practical considerations necessary for accurate in-liquid imaging.

Nanoscale corrosion behaviour of copper wire fabricated on silicon wafer using OL-EPM

Corrosion of copper (Cu) fine wires is a critical issue in semiconductor device fabrication, where transient exposure to dilute electrolytes during processing can

Figure 1

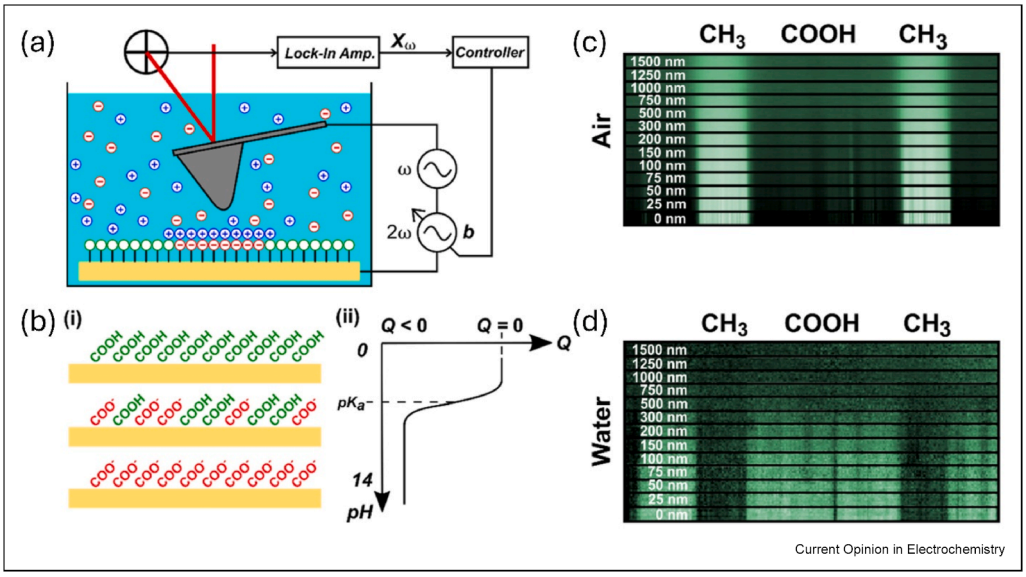

(a) AC-KPFM in aqueous solution: The cantilever deflection amplitude X_ω, induced by electrostatic forces from ions, is nulled by adjusting the AC bias amplitude *b*. **(b)** Surface charge modulation via pH: At low pH (~0), carboxyl groups are mostly protonated (Q ≈ 0); at high pH (~14), they are deprotonated (Q < 0). The Q–pH inflection point defines the effective pKa. **(c, d)** Impact of tip-sample distance. Surface potential measured by AC-KPFM on a COOH/CH_3 sample in **(c)** air and **(d)** deionized water for different lift heights. Adapted with permission [10]. Copyright 2022, American Chemical Society.

lead to nanoscale defects [33]. Understanding where and how local corrosion cells initiate is essential for developing prevention strategies. In a prior study by Honbo et al. employed OL-EPM to investigate structural and ESP changes on 2 μm Cu wires formed on a Si wafer, immersed in 10 μM NaCl solution [30] (Figure 2a). Initial topographic and ESP images showed nanoscale variations, indicating pre-existing corrosion from sample preparation (Figure 2b). After 63 min of immersion, significant surface dissolution was observed. Importantly, regions that initially exhibited higher ESP (anodic) had corroded more, while lower-ESP regions (cathodic) remained more stable. This confirmed that localized anodic sites drive corrosion (Figure 2b). It is important to note that during a corrosion process, positive current flows from anodic to cathodic areas through the electrolyte. As a result, the electric potential near the anodic region in solution is expected to be higher than near the cathodic region. These results demonstrate the capability of OL-EPM to directly correlate nanoscale ESP variations with localized anodic and cathodic activity, providing powerful, real-time insight into the initiation of corrosion processes in microelectronic structures.

Nanoscale corrosion observation of sensitized duplex stainless steel using OL-EPM

Duplex stainless steel, composed of roughly equal ferrite (α) and austenite (γ) phases, is widely used in harsh environments, such as nuclear, desalination, and chemical plants, due to its superior corrosion resistance [34–36]. However, assessing localized corrosion is challenging, as detectable effects may take months to appear, rendering conventional imaging methods (e.g., scanning electron microscopy (SEM), AFM, and scanning tunneling microscopy (STM)) inefficient. Operando OL-EPM reveals its capability to provide real-time, nanoscale monitoring of corrosion-prone sites, linking local ESP variations to eventual material degradation before visible damage occurs.

To overcome this, operando OL-EPM was employed to study the corrosion behavior of duplex stainless steel (UNS S32750), particularly in weld-sensitized regions where corrosion resistance degrades [30]. Optical microscopy revealed that welding significantly enlarged ferrite grains in the heat-affected zone (Figure 2c). OL-EPM enabled nanoscale monitoring of corrosion at various distances from the weld (data shown for P1), offering practical, real-time insight into local corrosion behavior. Time-lapse ESP imaging revealed that regions with initially elevated surface potential (visible at 37 min) underwent progressive selective dissolution, forming topographic depressions by 144 min (Figure 2d). These depressions aligned with the original high-ESP regions, demonstrating OL-EPM's predictive ability to identify corrosion-prone sites before visible damage emerges. Overall,

Figure 2

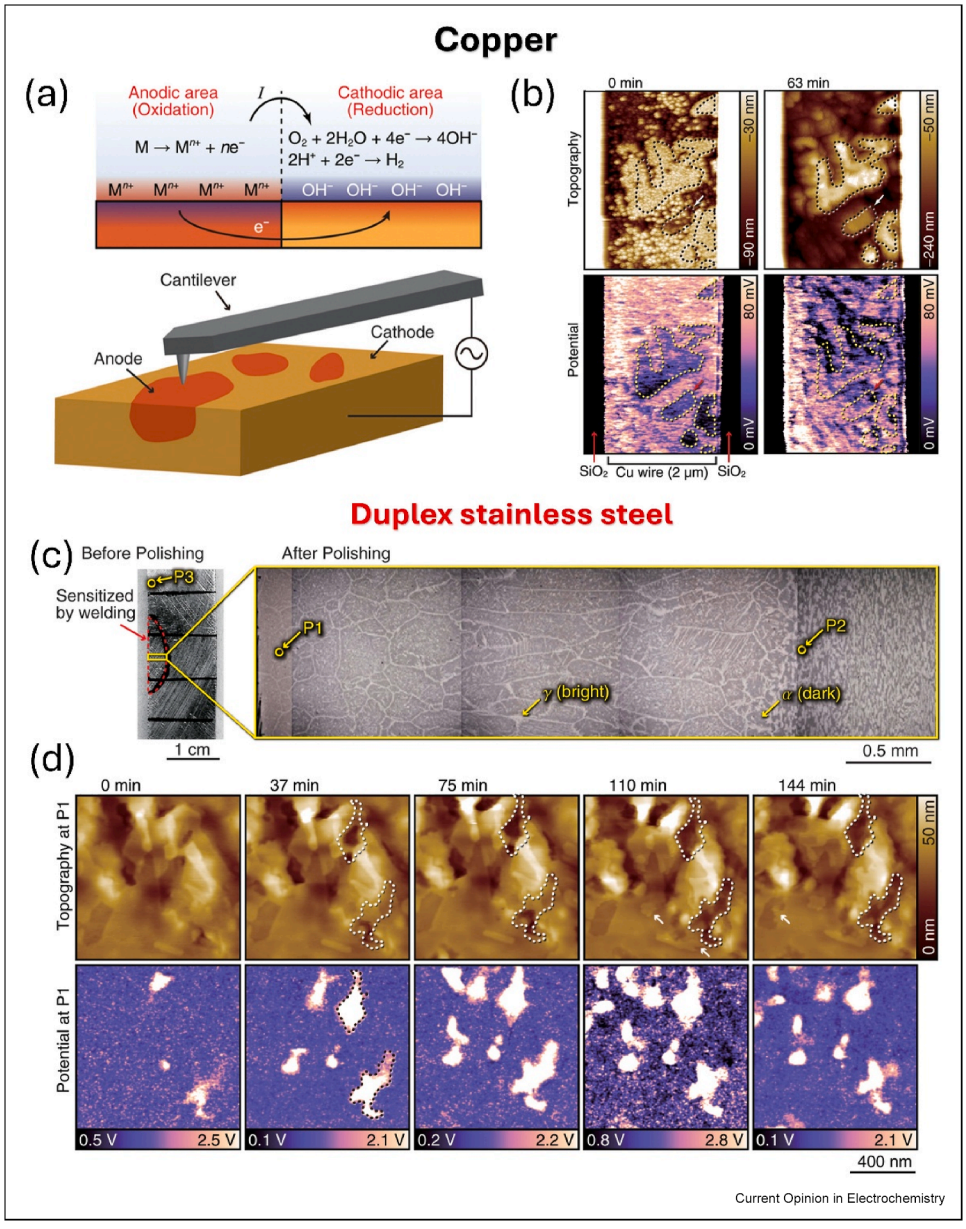

(a) Schematic representations indicating typical corrosion reactions and OL-EPM measurement of local corrosion cells. **(b)** Topographic and surface potential images of a 2 μm copper wire acquired using OL-EPM in a 10 μM NaCl solution (V_{ac} = 0.3 V, f_1 = 700 kHz, f_2 = 730 kHz). "0 min" denotes the start of imaging for this region. The "0 min" reference in the height scale approximately corresponds to the average height of the insulating SiO_2 regions. For consistent comparison across the time series, the lower-potential areas identified at 0 min are marked by dotted lines in all subsequent images. **(c)** Optical micrographs of the duplex stainless-steel sample used in this study. Low-magnification image of the as-received surface before polishing. The region outlined by dotted lines indicates the weld-sensitized zone. Higher-magnification image of the same region after mechanical polishing, corresponding to the rectangular area. OL-EPM measurements were carried out at positions P1–P3 within this area. **(d)** Topographic and potential images of the sensitized duplex stainless steel were obtained in a 10 mM NaCl solution at point P1 under the conditions V_{ac} = 1 V, f_1 = 700 kHz, and f_2 = 730 kHz. The time "0 min" corresponds to the moment imaging of this area began. Note that the 0 nm reference in the topographic images is arbitrary. Adapted with permission [30]. Copyright 2016, American Chemical Society.

these results highlight how welding-induced microstructural changes increase corrosion susceptibility and how OL-EPM enables early detection at the nanoscale.

Detecting nanoscale carbon-based overcoat defects using OL-EPM

Cobalt-based hard disk media (HDM) is a key component in hard disk drives (HDDs) [37]. To enhance

HDD durability, a carbon-based overcoat (COC) is applied to protect the HDM surface [38]. However, increasing recording density requires reducing the spacing between the HDM and the magnetic head, driving demand for thinner COC layers (Figure 3a) [39]. Thinning the COC can lead to local defects that expose the HDM, initiating corrosion when water adsorbs onto these defects. Therefore, reducing COC thickness without compromising coverage is critical to prevent corrosion while increasing HDD capacity. OL-EPM directly addresses this challenge by detecting nanoscale defects and mapping ESP variations linked to localized electrochemical activity, thereby enabling early identification of corrosion-susceptible regions in protective coatings.

In a study by Hirata et al., an OL-EPM was used to measure the topography and ESP distribution of two HDMs with different COC thicknesses in dilute HNO_3 solution (Figure 3b) [40]. The topographic images of two various COC thicknesses, including T1 (2.71 nm) and T2 (2.62 nm) showed surface corrugations (∼20 nm in

Figure 3

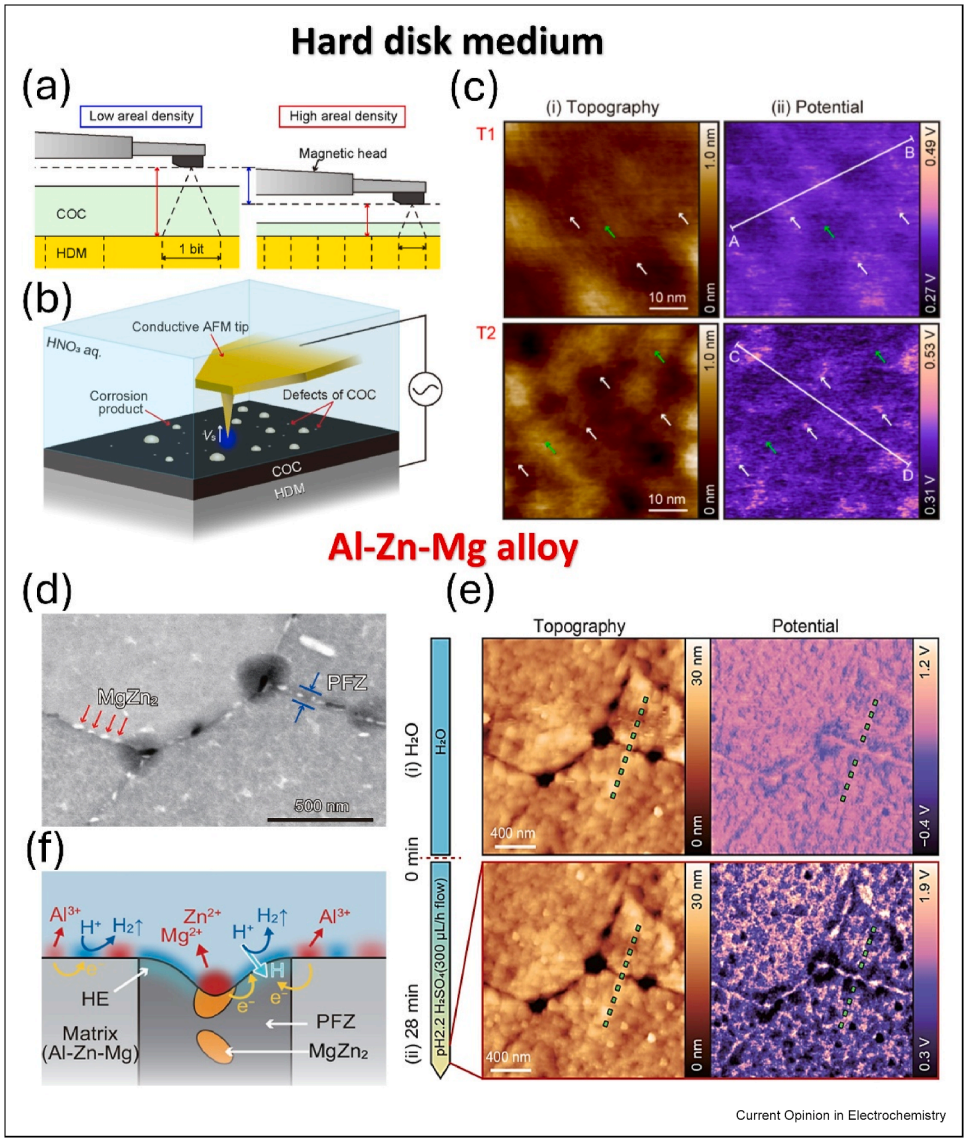

(a) The principle behind enhancing the areal storage density of a hard disk medium (HDD); **(b)** OL-EPM measurements performed on the carbon overcoat (COC) and hard disk medium (HDM); **(c)** High-resolution (i) topographic and (ii) potential images of the T1 and T2 samples obtained by OL-EPM in 1 mM HNO_3 solution (*Vac* = 0.8 V, *f*1 = 700 kHz, *f* 2 = 800 kHz). Adapted with permission [40]. Copyright 2024, American Chemical Society. **(d)** SEM image plus **(e)** OL-EPM measurements performed at the GB in water and a pH 2.2 H_2SO_4 solution, indicating topographic and surface potential images. (Measurement conditions: V_{ac} = 800 mV, f_1 = 700 kHz, f_2 = 800 kHz). **(f)** A possible model to describe the corrosion mechanism at GB, indicating anodic dissolution of the $MgZn_2$ precipitates. Adapted with permission [41]. Copyright 2023, American Chemical Society.

Table 1

Comparative overview of Kelvin probe techniques: SKP, KPFM, AC-KPFM, and OL-EPM.

Feature	SKP	KPFM	AC-KPFM	OL-EPM
Scale	Macroscopic	Nanoscopic	Nanoscopic	Nanoscopic
Probe size	Micro to millimeter tip radius	Nanometer tip radius	Nanometer tip radius	Nanometer tip radius
Operating environment	Moist surface, thin water film, or large droplet	Dry, ambient, or vacuum	Liquid or humidified	Liquid or humidified
Spatial resolution	Micro to millimeter	Nanometer	Nanometer	Nanometer
Feedback mechanism	DC feedback	DC feedback	Closed-loop, AC voltage of twice the frequency (2ω)	Open-loop, frequencies of ω and 2ω
Limitations	Must consider oxide resistivity, film thickness, and relative humidity (RH)	Usually not electrochemical; sensitive to surface work function, dipoles, and charges	Requires frequency optimization to suppress Faradaic reactions; measures relative, not absolute ESP	Requires frequency optimization to suppress Faradaic reactions; measures relative, not absolute ESP

lateral size), reflecting the underlying magnetic layer's texture [37] (Figure 3c). Importantly, the ESP images revealed nanoscale regions of elevated ESP, particularly at grain boundaries, suggesting these sites are prone to COC defects and anodic dissolution (Figure 3c). The ESP maps showed that potential variations in the thinner COC sample (T2) reached ∼100 mV, compared to ∼60 mV in T1. This indicates that T2 experienced more active corrosion, consistent with expectations for thinner, more defect-prone coatings.

Nanoscale corrosion observation at grain boundaries of Al–Zn–Mg alloy using OL-EPM

Localized corrosion in aluminum (Al)-based alloys is primarily driven by microgalvanic coupling from microstructural inhomogeneities such as grain boundaries (GBs) and intermetallic particles [42,43]. In Al–Zn–Mg alloys, GBs often host $MgZn_2$ precipitates, flanked by precipitate-free zones (PFZs) of pure Al (30–500 nm wide) [44], forming nanoscale electrochemical cells that promote corrosion. While this model is widely supported, the real-time spatial evolution of corrosion cells at GBs has remained unclear, and existing theories do not fully explain the transition to large-scale pit formation after $MgZn_2$ dissolution. By directly tracking nanoscale corrosion dynamics in real time, OL-EPM bridges this gap, linking microstructural features to local ESP variations associated with electrochemical activity, and thereby revealing the early stages of intergranular corrosion and pitting initiation.

In a landmark study, Yamamoto et al. used OL-EPM to track corrosion dynamics of Al–Zn–Mg alloys in H_2SO_4 (pH 2.2), observing the same regions imaged via SEM (Figure 3d) [41]. Initial OL-EPM scans in pure water (not very corrosive) revealed GB depressions in topography and line-shaped low-ESP regions aligning with PFZs (Figure 3e–(i)), suggesting PFZs act as cathodic zones, while $MgZn_2$ and Al matrix regions are anodic (Figure 3f). Upon exposure to acidic solution, ESP contrast intensified dramatically (Figure 3e–(ii)), with anodic spots forming along GBs and distinct surrounding cathodic zones. Notably, topography remained largely unchanged, confirming these shifts reflect true electrochemical activity rather than geometric artifacts. This study offers real-time insight into corrosion cell evolution and refines the mechanistic understanding of pitting initiation in Al–Zn–Mg alloys.

Conclusions and perspectives

In-situ surface potential techniques, particularly AC-KPFM and OL-EPM, have significantly advanced nanoscale ESP imaging for electrochemistry and corrosion science. Unlike traditional DC-KPFM, limited to dry environments and electrostatic interpretation, these methods enable direct, non-invasive mapping of ESP under fully immersed or humid conditions, key to capturing realistic corrosion evolution. OL-EPM excels in detecting localized anodic/cathodic activity at grain boundaries, phases, and intermetallics without tip bias or Faradaic interference. AC-KPFM, using high-frequency excitation, stabilizes measurements in reactive electrolytes by minimizing electrochemical reactions. Together, they bridge high spatial resolution with electrochemical insight. Challenges include the lack of standardized calibration, complex signal interpretation due to hydration layers and oxides, and inconsistent protocols for probe design and electrolyte control. Future progress will depend on.

- Establishing standardized protocols for tip–sample operation to reliably distinguish electrostatic from redox signals.
- Integration with operando spectroscopy (e.g., in-situ Raman, IR, X-ray photoelectron spectroscopy (XPS)) to provide complementary chemical insight.
- Developing chemically robust probes, such as doped-silicon/silicon nitride [45], PtSi [46], and conductive doped diamond [47] tips which could withstand aggressive electrolytes and extend operational lifetimes.
- Incorporating machine learning approaches for automated defect recognition, noise reduction, and real-time data interpretation, drawing inspiration from recent advances in artificial intelligence (AI)-enabled scanning probe microscopy [48,49].
- Advancing multiphysics modeling to link experimental ESP maps with predictive electrochemical simulations of localized corrosion [5].

In short, AC-KPFM and OL-EPM are emerging as indispensable tools for mechanistic insight into corrosion and interfacial chemistry at the nanoscale. With improved probe design, standardized protocols, and integration of machine learning–driven analysis, these techniques hold promise to evolve from specialized research tools into broadly applicable platforms for automated, real-time nanoscale electrochemistry.

Declaration of competing interest

The author declares that he has no known competing financial interests or personal relationships that could have appeared to influence the work reported in this paper.

Acknowledgements

E. Rahimi gratefully acknowledges his affiliation with TU Delft during the preparation of this work and appreciates the institutional support and access to scientific resources that facilitated its development. This work was carried out independently and did not utilize project-specific funding or laboratory infrastructure.

Data availability

Data will be made available on request.

References

Papers of particular interest, published within the period of review, have been highlighted as:

* of special interest
** of outstanding interest

1. Stampfl C, Veronica Ganduglia-Pirovano M, Reuter K, Scheffler M: **Catalysis and corrosion: the theoretical surface-science context**. *Surf Sci* 2002, **500**:368–394.

2. Sadewasser S, Glatzel T: *Kelvin probe force microscopy*. Springer; 2012.

3. McCafferty E: *Introduction to corrosion science*. Springer Science & Business Media; 2010.

4. Jadhav N, Gelling VJ: **Review—the use of localized electrochemical techniques for corrosion studies**. *J Electrochem Soc* 2019, **166**, C3461.

5. Collins L, Kilpatrick JI, Kalinin SV, Rodriguez BJ: **Towards nanoscale electrical measurements in liquid by advanced KPFM techniques: a review**. *Rep Prog Phys* 2018, **81**, 086101.

6. Rahimi E, Palacios-Corella M, Mol A, Pané S, Puigmartí-Luis J. Kelvin probe force microscopy in bionanotechnology: current advances and future perspectives. Adv Mater.n/a:e10671.

7. Rohwerder M, Turcu F: **High-resolution Kelvin probe microscopy in corrosion science: scanning Kelvin probe force microscopy (SKPFM) versus classical scanning Kelvin probe (SKP)**. *Electrochim Acta* 2007, **53**:290–299.

8. Lenton ICD, Pertl F, Shafeek L, Waitukaitis SR: **Beyond the blur: using experimentally determined point spread functions to improve scanning Kelvin probe imaging**. *J Appl Phys* 2024, **136**.

9. Nazarov A, Thierry D: **Application of scanning Kelvin probe in the study of protective paints**. *Front Mater* 2019, **6**:192.

10. ** Hackl T, Schitter G, Mesquida P: **AC Kelvin probe force microscopy enables charge mapping in water**. *ACS Nano* 2022, **16**:17982–17990.
Presents a novel implementation of AC-KPFM for high-resolution charge mapping in aqueous environments, significantly enhancing its applicability to corrosion, electrochemical, and biological systems.

11. Melitz W, Shen J, Kummel AC, Lee S: **Kelvin probe force microscopy and its application**. *Surf Sci Rep* 2011, **66**:1–27.

12. Liscio A, Palermo V, Samorì P: **Nanoscale quantitative measurement of the potential of charged nanostructures by electrostatic and Kelvin probe force microscopy: unraveling electronic processes in complex materials**. *Accounts Chem Res* 2010, **43**:541–550.

13. Qin T-X, You E-M, Zhang M-X, Zheng P, Huang X-F, Ding S-Y, *et al.*: **Quantification of electron accumulation at grain boundaries in perovskite polycrystalline films by correlative infrared-spectroscopic nanoimaging and Kelvin probe force microscopy**. *Light Sci Appl* 2021, **10**:84.

14. Kharitonov DS, Örnek C, Claesson PM, Sommertune J, Zharskii IM, Kurilo II, Pan J: **Corrosion inhibition of aluminum alloy AA6063-T5 by Vanadates: microstructure characterization and corrosion analysis**. *J Electrochem Soc* 2018, **165**, C116.

15. Esfahani Z, Rahimi E, Sarvghad M, Rafsanjani-Abbasi A, Davoodi A: **Correlation between the histogram and power spectral density analysis of AFM and SKPFM images in an AA7023/AA5083 FSW joint**. *J Alloys Compd* 2018, **744**:174–181.

16. Zhu Y, Sun K, Frankel GS: **Intermetallic phases in aluminum alloys and their roles in localized corrosion**. *J Electrochem Soc* 2018, **165**, C807.

17. Andreatta F, Apachitei I, Kodentsov AA, Dzwonczyk J, Duszczyk J: **Volta potential of second phase particles in extruded AZ80 magnesium alloy**. *Electrochim Acta* 2006, **51**:3551–3557.

18. Hu Z, Yin Z, Yin Z, Wang K, Liu Q, Sun P, *et al.*: **Corrosion behavior characterization of as extruded Mg-8Li-3Al alloy with minor alloying elements (Gd, Sn and Cu) by scanning Kelvin probe force microscopy**. *Corros Sci* 2020, **176**, 108923.

19. Imani A, Rahimi E, Lekka M, Andreatta F, Magnan M, Gonzalez-Garcia Y, *et al.*: **Albumin protein Impact on early-stage in vitro biodegradation of magnesium alloy (WE43)**. *ACS Appl Mater Interfaces* 2024, **16**:1659–1674.

20. Yuan R, Gu Y, Wu H: **Effect of surface Volta potential of Cr-containing steel on uniform corrosion and pitting corrosion**. *Mater Corros* 2021, **72**:1774–1786.

21. Murase Y, Masuda H, Katayama H: **Corrosion resistance of finer/coarser pearlitic structures of carbon steel**. *J Electrochem Soc* 2021, **168**, 041501.

22. Li G, Li Z, Rahimi E, Muratori M, Smith A, Navarro MJS, Gonzalez-Garcia Y: **Pit initiation in quenching and partitioning processed martensitic stainless steels**. *Electrochim Acta* 2024, **498**, 144646.

23. Örnek C, Leygraf C, Pan J: **Passive film characterisation of duplex stainless steel using scanning Kelvin probe force microscopy in combination with electrochemical measurements**. *npj Mater Degrad* 2019, **3**:8.

24. Rahimi E, Kosari A, Hosseinpour S, Davoodi A, Zandbergen H, Mol JMC: **Characterization of the passive layer on ferrite and austenite phases of super duplex stainless steel**. *Appl Surf Sci* 2019, **496**, 143634.

25. Örnek C, Leygraf C, Pan J: **On the Volta potential measured by SKPFM–fundamental and practical aspects with relevance to corrosion science**. *Corrosion Eng Sci Technol* 2019, **54**: 185–198.

26. Rahimi E, Offoiach R, Lekka M, Fedrizzi L: **Electronic properties and surface potential evaluations at the protein nanobiofilm/oxide interface: Impact on corrosion and biodegradation**. *Colloids Surf B Biointerfaces* 2022, **212**, 112346.

27. Rahimi E, Offoiach R, Baert K, Terryn H, Fedrizzi L, Lekka M: **Albumin protein adsorption on CoCrMo implant alloy: Impact on the corrosion behaviour at localized scale**. *J Electrochem Soc* 2022, **169**, 031507.

28. Yan Y, Yang H, Su Y, Qiao L: **Study of the tribocorrosion behaviors of albumin on a cobalt-based alloy using scanning Kelvin probe force microscopy and atomic force microscopy**. *Electrochem Commun* 2016, **64**:61–64.

29. * Rahimi E, Imani A, Lekka M, Andreatta F, Gonzalez-Garcia Y, Mol JMC, *et al.*: **Morphological and surface potential characterization of protein nanobiofilm formation on magnesium alloy oxide: their role in biodegradation**. *Langmuir* 2022, **38**: 10854–10866.
Links protein film morphology and surface potential to localized electrochemical responses, showing how KPFM helps unravel biodegradation evolutions.

30. Honbo K, Ogata S, Kitagawa T, Okamoto T, Kobayashi N, Sugimoto I, *et al.*: **Visualizing nanoscale distribution of corrosion cells by open-loop electric potential microscopy**. *ACS Nano* 2016, **10**:2575–2583.

31. Checa M, Fuhr AS, Sun C, Vasudevan R, Ziatdinov M, Ivanov I, *et al.*: **High-speed mapping of surface charge dynamics using sparse scanning Kelvin probe force microscopy**. *Nat Commun* 2023, **14**:7196.

32. Zhou K, Chen J, Wang T, Su Y, Qiao L, Yan Y: **Effect of surface energy on protein adsorption behaviours of treated CoCrMo alloy surfaces**. *Appl Surf Sci* 2020, **520**, 146354.

33. Kodera M, Uekusa S-i, Nagano H, Tokushige K, Shima S, Fukunaga A, *et al.*: **Stress corrosion cracking of Cu interconnects during CMP with a Cu/porous low-k structure**. *J Electrochem Soc* 2005, **152**, G506.

34. Rahimi E, Rafsanjani-Abbasi A, Davoodi A, Hosseinpour S: **Characterization of the native passive film on ferrite and austenite phases of sensitized 2205 duplex stainless steel**. *J Electrochem Soc* 2019, **166**, C609.

35. Yao J, Qi Z, Dong C: **Real-time evolution and characterization of passive films on individual ferrite and austenite phases of duplex stainless steel**. *Electrochem Commun* 2022, **137**, 107265.

36. Ye Z, Guan L, Li Y, Zhong J, Liao L, Xia D, Huang J: **Understanding the galvanic corrosion of Cu-Ni alloy/2205 DSS couple using electrochemical noise and microelectrochemical studies**. *Corros Sci* 2023, **224**, 111512.

37. Dwivedi N, Ott AK, Sasikumar K, Dou C, Yeo RJ, Narayanan B, *et al.*: **Graphene overcoats for ultra-high storage density magnetic media**. *Nat Commun* 2021, **12**:2854.

38. Dwivedi N, Satyanarayana N, Yeo RJ, Xu H, Ping Loh K, Tripathy S, Bhatia CS: **Ultrathin carbon with interspersed graphene/fullerene-like nanostructures: a durable protective overcoat for high density magnetic storage**. *Sci Rep* 2015, **5**, 11607.

39. Marchon B, Pitchford T, Hsia Y-T, Gangopadhyay S: **The head-disk interface roadmap to an areal density of 4 Tbit/in2**. *Adv Tribol* 2013, **2013**, 521086.

40. ** Hirata K, Omi J-i, Taniguchi D, Miyazawa K, Komatsu F, Takahashi Y, Fukuma T: **Corrosion inspection for hard disk media with carbon-based overcoats by in-liquid open-loop electric potential microscopy**. *ACS Appl Mater Interfaces* 2024, **16**:70020–70027.
Applies in-liquid OL-EPM to assess corrosion in magnetic storage media, opening a new avenue for non-destructive inspection in microelectronics.

41. * Yamamoto S, Taniguchi D, Okamoto T, Hirata K, Ozawa T, Fukuma T: **Nanoscale corrosion mechanism at grain boundaries of the Al–Zn–Mg alloy investigated by open-loop electric potential microscopy**. *J Phys Chem C* 2023, **127**: 5281–5288.
Reveals localized corrosion mechanisms at grain boundaries using high-resolution OL-EPM, critical for alloy development.

42. Kosari A, Tichelaar F, Visser P, Zandbergen H, Terryn H, Mol JMC: **Dealloying-driven local corrosion by intermetallic constituent particles and dispersoids in aerospace aluminium alloys**. *Corros Sci* 2020, **177**, 108947.

43. * Bartawi EH, Marioara CD, Shaban G, Rahimi E, Mishin OV, Sunde JK, *et al.*: **Effects of grain boundary chemistry and precipitate structure on intergranular corrosion in Al-Mg-Si alloys doped with Cu and Zn**. *Corros Sci* 2024, **236**, 112227.
Links micro and nano-chemical variations at grain boundaries to intergranular corrosion susceptibility, emphasizing microstructural control in alloy design.

44. Jiang K, Lan Y, Pan Q, Deng Y: **Effect of the Zn/Mg ratio on microstructures, mechanical properties and corrosion performances of Al-Zn-Mg alloys**. *Materials* 2020, **13**:3299.

45. Efaw CM, da Silva T, Davis PH, Li L, Graugnard E, Hurley MF: **Toward improving ambient volta potential measurements with SKPFM for corrosion studies**. *J Electrochem Soc* 2019, **166**, C3018.

46. Nadaud K, Nataf GF, Jaber N, Bah M, Negulescu B, Andreazza P, *et al.*: **Subcoercive field dielectric response of 0.5(Ba0.7Ca0.3TiO3)-0.5(BaZr0.2Ti0.8O3) thin film: peculiar third harmonic signature of phase transitions and residual ferroelectricity**. *Appl Phys Lett* 2024, **124**.

47. Liu X, Lu X, Lang X, Li M, Gou Y, Jiang Y, *et al.*: **Direct measurement of carrier distribution in perovskite by scanning capacitance microscopy**. *J Phys Chem C* 2025, **129**:648–657.

48. Diao Z, Ueda K, Hou L, Li F, Yamashita H, Abe M: **AI-equipped scanning probe microscopy for autonomous site-specific atomic-level characterization at room temperature**. *Small Methods* 2025, **9**, 2400813.

49. Krull A, Hirsch P, Rother C, Schiffrin A, Krull C: **Artificial-intelligence-driven scanning probe microscopy**. *Commun Phys* 2020, **3**:54.